Vortical and acoustical mode coupling inside a two-dimensional cavity with transpiring walls

Joseph Majdalani
Mechanical and Industrial Engineering Department, Marquette University, Milwaukee, Wisconsin 53233

(Received 26 May 1998; revised 12 March 1999; accepted 23 March 1999)

In a long, low aspect ratio, two-dimensional cavity, where gaseous motion is permitted along transpiring walls, a time-dependent field is established when low amplitude, sinusoidal pressure oscillations with nonzero mean are introduced. An accurate solution is extracted here for the time-dependent field by way of small parameter perturbations. Contingent upon small pressure-wave amplitudes, Navier–Stokes equations are linearized to the order of the mean flow Mach number to furnish interaction equations governing the unsteady field. The latter is decomposed into acoustic and solenoidal fields coupled through Dirichlet-type boundary conditions. Solving for the solenoidal field from the momentum equation employs separation of variables and multiple scale expansions based on a careful choice of an inner scale. In fact, the unique inner scale used in the two-variable derivative expansion method is original in the sense that it stems from an unconventional, nonlinear variable transformation. A uniformly valid solution is formulated subsequently for the temporal field. This explicit solution discloses the character of the acoustic boundary layer evolving from damped traveling waves. The rate of decay is found to depend on a viscosity parameter, revealing that deeper penetration of rotational waves is possible at low viscosity. Characterization of the boundary layer region is covered in addition to a standard error analysis. In closing, results are verified through comparisons to accurate numerical predictions. [S0001-4966(99)00907-8]

PACS numbers: 43.20.Hc, 43.20.Mv, 43.28.Py [LCS]

INTRODUCTION

When harmonic disturbances are introduced inside a rectangular cavity with transpiring walls, a rotational component of the time-dependent velocity is produced along with the plain, irrotational, acoustic field. The resulting time-dependent field can be difficult to analyze since it must include the influence of the steady flow component. The traditional approach to resolve the resulting coupled equations is paved with numerous mathematical obstructions that prevent exacting analytical solutions in finite form. Based on a technique used recently by the author,[1] an assault on the problem will be attempted here. The method relies heavily on regular and multiple scale perturbation tools, making use of naturally occurring similarity parameters that happen to be small quantities. By way of example, in linearizing the Navier–Stokes equations, the ratio of the acoustic-to-mean pressure amplitude will be used as a primary perturbation parameter. The Mach number at the transpiring wall will be found to be another instrumental perturbation parameter that is frequently encountered. Later, in resolving the solenoidal field, a small parameter reminiscent of the Stokes number will recur, providing a gauge to expand the solenoidal velocity in a series of progressively diminishing terms.

The originality of this work stems from the mathematical treatment of the interaction equations developed for the time-dependent field. This treatment involves a singular boundary value problem whose solution features a novel scaling transformation. In previous work, Majdalani and Van Moorhem[1] have tackled a similar problem involving unsteady axisymmetric motion inside a cylindrical tube and different boundary conditions. The former analysis employed the so-called ''composite-scale technique,'' a hybrid perturbation method that involved reducing three spatial length scales into one, nonunique, composite-scale function, before applying the derivative expansion method. The current methodology does not invoke composite-scale matching, but rather standard perturbation tools. In the process, one unique virtual scale will be identified as the outcome of a nonlinear variable transformation. To the author's knowledge, the nonlinear transformation that will be presented has not been addressed previously in multiple scale analysis. Contrary to the ad hoc approach employed previously by Majdalani and Van Moorhem,[1] a mathematically rigorous approach will be invested here in constructing the uniformly valid asymptotic formulation.

The practical motivation stems, in part, from the need to obtain an approximate solution for the time-dependent field that can be helpful in explaining and elucidating observations reported by Ma[2–4] and Barron[5] in two experimental investigations that involved a two-dimensional geometry. In both instances, sublimating carbon dioxide originating from the flat surface of heated blocks of dry ice was used to simulate the transpiring gas inside a long, segmented, rectangular chamber. In both cases, harmonic pressure waves were produced by means of a variable speed, reciprocating piston. In Barron's apparatus, a Scotch-yoke mechanism was used to drive the piston by imparting a purely sinusoidal motion at a well-prescribed frequency, a substantial improvement over Ma's slider-crank mechanism which could only approximate sinusoidal motions. In any event, both investigations suffered from a lack of applicable analytical models, a problem that is hoped to be remedied in the present development.

For the purpose of attaining a reliable solution, the paper starts in Sec. I with a brief description of the two-

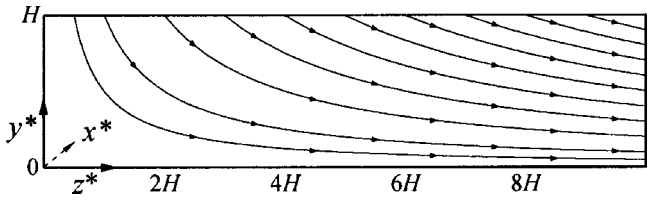

FIG. 1. Chamber half-space showing mean flow streamlines. In the orthogonal coordinate system indicated, the x^* axis is perpendicular to the plane of view, y^* is the normal distance measured from the rigid wall, and z^* is the axial distance measure from the head end.

dimensional geometry and bulk fluid motion, along with a statement of the fundamental criteria whose violation is inadmissible. This is followed in Sec. II by a formulation of the linearized Navier–Stokes equations which rests on decomposing variables into mean and small time-dependent fluctuations. In the process, interaction equations that incorporate the influence of the mean flow are derived for the time-dependent field to the order of the surface Mach number. In Sec. III, the classical mean flow velocity established inside a rectangular cavity is analyzed. The time-dependent field is decomposed in Sec. IV into acoustic, irrotational, pressure-driven, and rotational, solenoidal, vorticity-driven elements. Equations governing each set are produced along with pertinent boundary conditions. Unlike the acoustic set which can be readily resolved, the solenoidal set demands a special treatment and is conveniently deferred to a separate section. Hence, in Sec. V, separation of variables accompanies a careful scaling analysis in the development of a uniformly valid solution to the rotational field. Attempts to elucidate particular features of the new finding and to explain its impact on the overall time-dependent solution are undertaken in Sec. VI where the time-dependent boundary layer is characterized. The global error associated with the analytical formulation is evaluated and the order of the truncation error is established. Throughout this study, verifications are made at various stages by comparing analytical predictions to reliable computational data. By way of closing, several conclusions are reiterated in Sec. VII.

I. PROBLEM FORMULATION

We begin by describing the idealized geometry along with important criteria that must be met for the mathematical model to hold.

A. Geometry

The two-dimensional acoustic field is considered in the half-space of a long rectangular cavity of length L, width W, and height $H(W \gg H, L \gg H)$, with one acoustically compliant membrane (simulating a transpiring wall), through which mean transmission of a gas (of kinematic viscosity v_0) occurs at a steady blowing speed of V_b. Gas entering the chamber at $y^*=H$ is led to change course, swerve, and head downstream. As represented schematically in Fig. 1, the chamber is acoustically hard at the head end ($z^*=0$). The sound field under investigation is choked at the downstream end due to a constriction in flow area (not shown). In addition, the lateral walls normal to the x^* axis are impenetrable (note that the x^* axis is perpendicular to the plane of view in Fig. 1). Since the chamber width is larger than its height, variations in the x^* direction are ignored. Under idealized conditions, the flow is perfectly symmetrical about the central plane $y^*=0$. Taking advantage of symmetry, the domain investigation is limited to the half-space extending from the compliant wall to the central plane.

Superimposed on the mean fluid motion, a two-dimensional time-harmonic acoustic field of small amplitude (frequency ω_0 and pressure amplitude A_p) is admitted. This acoustic environment can be induced externally or triggered naturally from internally propagating pressure disturbances. In the forthcoming analysis, details of the acoustic source will not be addressed.

B. Principal criteria

In order to pursue a theoretical formulation of the time-dependent field, standard perturbation tools are implemented in conjunction with a fundamental assumption of a low mean flow Mach number of $O(10^{-3})$. In common nonreacting flows characterized by a typical speed of sound of 350 m/s, the low Mach number criterion casts a limit of 2 m/s on the mean flow speed. In reality, this upper threshold for the Mach number is not too restrictive since, in many applications, it corresponds to a condition of intense mean flow transmission known as ''hard blowing.'' Another basic assumption that must be tolerated to manage a solution constrains the acoustic pressure amplitude A_p to remain small by comparison to the mean pressure p_0 at the chamber head end. The latter must be uniform in order to maintain rigor and consistency in comparing terms of various orders of magnitude arising in the perturbation process which rests strongly on the pressure wave amplitude, A_p/p_0, a gauge to which other quantities are compared. This criterion is found to be contingent upon a geometrical restriction of $L/H < 100$. When these criteria are met, the forthcoming analysis will be seen to be applicable everywhere except near the choked end ($z^*=L$).

II. EQUATIONS OF MOTION

A standard normalization and small parameter linearization of the governing equations precedes the development of the interaction equations.

A. Conservation laws

Invoking Stokes' hypothesis of zero bulk viscosity, assuming constant viscosity, and disallowing body forces, conservation of mass and momentum can be cast in dimensionless form into

$$\frac{\partial \rho}{\partial t} + \nabla .(\rho \mathbf{u}) = 0, \tag{1}$$

$$\rho \frac{D\mathbf{u}}{Dt} = -\frac{\nabla p}{\gamma} + \frac{1}{\mathrm{Re}}\left[\frac{4}{3}\nabla(\nabla \cdot \mathbf{u}) - \nabla \times (\nabla \times \mathbf{u})\right], \tag{2}$$

where density ρ and pressure p are normalized by their mean values, ρ_0 and p_0, at the chamber head end, velocities are normalized by the chamber's intrinsic speed of sound a_0,

spatial coordinates (x, y, z) are the laboratory coordinates (x^*, y^*, z^*) normalized by H, and time $t(=a_0 t^*/H)$ is made dimensionless by referring t^* to the average time it takes for a pressure disturbance to travel from the compliant wall to the centerline, (H/a_0). The Reynolds number Re in Eq. (2) is $(a_0 H/v_0)$, γ is the ratio of specific heats, and $\mathbf{u}(y,z,t)$ is the total velocity, including both steady and unsteady components. Exacting the latter constitutes the main purpose of this article.

B. Approach

The procedure consists of decomposing the internal flow field into a steady and a time-dependent part. This is accomplished by writing each of the independent variables as a sum of their steady and time-dependent components. A small parameter perturbation scheme is suitable by virtue of the fundamental premise requiring the acoustic amplitude to be a small quantity relative to its mean counterpart.[6] In breaking the analysis into digestible pieces, we assume that the presence of time-dependent oscillations does not alter the general motion of the mean flow. This assumption can be later verified by realizing that terms that incorporate the time-dependent effects on the mean flow field are indeed secondary. Conversely, mean flow effects on the acoustic field are extraordinarily important and cannot be dismissed. Since superposition of the coupled elements is sought ultimately, equations that incorporate the coupling between steady and time-dependent components must be developed as well. Details are furnished below.

C. Variable decomposition

The local pressure can be expressed as the sum of its steady and acoustic components. Using, heretofore, asterisks to denote dimensional variables, and superscripts for perturbation orders, the dimensional pressure is split into

$$p^* = p^{*(0)}(y^*,z^*) + p^{*(1)}(y^*,z^*,t^*) = p^{*(0)} + A_p f(y^*,z^*)\cos(\omega_0 t^*), \tag{3}$$

where $p^{*(0)}$, subject to later verification, is taken to be a constant. In the time-dependent part of Eq. (3), A_p defines the acoustic pressure amplitude, and f is a normalized spatial function of $O(1)$. After normalizing by p_0, and substituting $p^{*(0)} \cong p_0$, Eq. (3) becomes

$$p = 1 + \epsilon_w f(y,z)\cos(\omega_0 t^*) = 1 + p^{(1)}(y,z,t), \tag{4}$$

where $\epsilon_w = A_p/p_0$ is the primary gauge parameter that provides a scale to which other terms can be compared. Density can be expanded in a similar way:

$$\rho(y,z,t) = \frac{\rho_0 + \rho^{*(1)}}{\rho_0} = 1 + \rho^{(1)}(y,z,t). \tag{5}$$

Velocity decomposition needs to be assessed carefully since its mean value is of the order of $V_b \mathbf{U}(y,z)$, where $\mathbf{U}(y,z)$ is a function of $O(1)$ to be described in Sec. III. Note that the term V_b defines the magnitude of the mean flow velocity crossing the plane $y=1$. Expanding the dimensional velocity into

$$\mathbf{u}^*(y,z,t) = V_b \mathbf{U}(y,z) + \mathbf{u}^{*(1)}(y,z,t), \tag{6}$$

we normalize by the chamber speed of sound a_0 and find that the nondimensional counterpart is of the order of the wall Mach number, M_b; the latter is a secondary perturbation parameter by virtue of $\epsilon_w < M_b \ll 1$. Note that ϵ_w remains very small, as defined in Eq. (4) and Sec. II B, being the amplitude of the small pressure disturbances normalized by the mean pressure. The dimensionless velocity becomes

$$\mathbf{u}(y,z,t) = M_b \mathbf{U}(y,z) + \mathbf{u}^{(1)}(y,z,t). \tag{7}$$

D. Interaction equations

Substituting Eqs. (4), (5), and (7) into Eqs. (1)–(2), one obtains, at the leading order expansion in the wave amplitude, a set for the steady flow motion:

$$\nabla . \mathbf{U} = 0, \tag{8}$$

$$\mathbf{U}.\nabla \mathbf{U} = \frac{1}{M_b \,\mathrm{Re}}\left[\frac{4}{3}\nabla(\nabla.\mathbf{U}) - \nabla\times(\nabla\times\mathbf{U})\right]. \tag{9}$$

Grouping terms that are comparable in magnitude to the first order in the wave amplitude, a linearized expansion of the interaction equations incorporating mean flow effects is attained:

$$\partial\rho^{(1)}/\partial t + \nabla.\mathbf{u}^{(1)} = -M_b \nabla.(\rho^{(1)}\mathbf{U}), \tag{10}$$

$$\frac{\partial \mathbf{u}^{(1)}}{\partial t} = M_b[\mathbf{u}^{(1)}\times(\nabla\times\mathbf{U}) + \mathbf{U}\times(\nabla\times\mathbf{u}^{(1)}) - \nabla(\mathbf{u}^{(1)}.\mathbf{U})] - \frac{\nabla p^{(1)}}{\gamma} + \frac{1}{\mathrm{Re}}\left[\frac{4}{3}\nabla(\nabla.\mathbf{u}^{(1)}) - \nabla\times(\nabla\times\mathbf{u}^{(1)})\right]. \tag{11}$$

Equations (10)–(11) reveal the intricate coupling between mean and time-dependent flow components which strongly affects the time-dependent solution character.

III. MEAN FLOW FIELD

When a classical mean flow stream function is assumed for the geometry at hand, both velocity and pressure distributions are determinable.

A. Velocity field

The velocity field $\mathbf{U}$ can be determined from the stream function $\mathbf{S}_f = \Psi \mathbf{e}_x$ obtained for a flow inside a rectangular cavity[7] where $\mathbf{U} = \nabla \times \mathbf{S}_f$. Using the classical stream function $\Psi(y,z) = -yz$, we have

$$\mathbf{U} = U_y \mathbf{e}_y + U_z \mathbf{e}_z = \frac{\partial \Psi}{\partial z}\mathbf{e}_y - \frac{\partial \Psi}{\partial y}\mathbf{e}_z = -y\mathbf{e}_y + z\mathbf{e}_z, \tag{12}$$

which does satisfy Eqs. (8)–(9).

B. Mean pressure correction

Having evaluated the velocity field from the stream function independently of mean pressure variations, one can use the steady momentum equation to deduce the pressure associated with the resulting field. Without incurring any loss

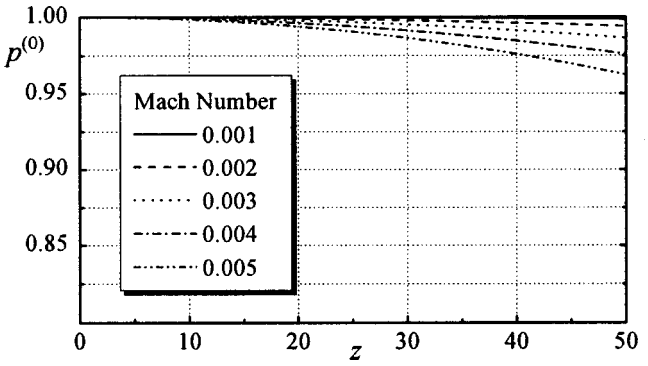

FIG. 2. Steady pressure distribution for practical mean flow Mach numbers.

in generality, one can set $p(y,z,t)=1+p_c(y,z)+p^{(1)}\times(y,z,t)$, where $p_c(y,z)$ is a spatial pressure correction term that we propose to determine. An auxiliary condition that must be met specifies that pressure at the chamber head end must be identical to the mean stagnation pressure where $p^{(0)}=1+p_c(0,0)=1$, or $p_c(0,0)=0$. The pertinent spatial correction can be obtained directly from Eq. (2) by direct substitution:

$$M_b\mathbf{U}.\nabla(M_b\mathbf{U})=-\frac{\nabla p_c}{\gamma}+\frac{1}{\mathrm{Re}}\times[\tfrac{4}{3}\nabla[\nabla.(M_b\mathbf{U})]-\nabla\times[\nabla(M_b\mathbf{U})]] \tag{13}$$

or

$$\nabla p_c/(\gamma M_b^2)=-\mathbf{U}.\nabla\mathbf{U}. \tag{14}$$

Equation (14) can be integrated to obtain, for $p_c(0,0)=0$, $p^{(0)}(y,z)=1-(\gamma/2)M_b^2(y^2+z^2)$; wherefrom

$$p^{(0)}(y,z)=1-(\gamma/2)M_b^2(y^2+z^2). \tag{15}$$

Note that in Eq. (15) the y-dependence can be safely ignored by comparison to the z-dependence, the former being smaller than unity, whereas z^2 varies from the order of unity to the order of 10^3. Additionally, since M_b is of $O(10^{-3})$, and z is less than 100, the error in assuming a constant steady pressure is insignificant, being of order $M_b^2z^2$. The corrected pressure distribution, shown in Fig. 2, indicates that axial pressure variations are indeed negligible except in very long chambers with large Mach numbers. Since the Mach number in the majority of cases does not exceed 0.005, the assumption of a uniform mean value needed to represent the steady pressure distribution is well justified. Having described the steady flow field character, its impact on the acoustic component is examined next.

IV. TIME-DEPENDENT FIELD

In order to resolve the effects of the steady field on the time-dependent field, the interaction equations are developed for small amplitude pressure and vorticity-driven disturbances inside the chamber. Proper boundary conditions are also examined.

A. Irrotational and solenoidal fields

The time-dependent velocity vector $\mathbf{u}^{(1)}$ is decomposed into two vectors of distinct characters, one that is irrotational and one that is solenoidal[8]

$$\mathbf{u}^{(1)}=\mathbf{u}_{\text{irrotational}}+\mathbf{u}_{\text{solenoidal}}=\hat{\mathbf{u}}+\tilde{\mathbf{u}} \tag{16}$$

contingent upon, $\nabla\times\hat{\mathbf{u}}=0$, and $\nabla\cdot\hat{\mathbf{u}}=0$. Similar decomposition of a small amplitude disturbance into two modes of fluctuations, a pressure mode and a vorticity mode, has been accomplished previously by numerous authors, including Chu and Kovásznay,[9] Carrier and Carlson,[10] and Flandro.[11]

Plugging Eq. (16) back into Eqs. (10)–(11), the interaction equations for small disturbances can be written for each of the modes. The total time-dependent velocity field can be constructed, thereafter, by superimposing the solution vectors linearly. Designating the irrotational mode variables by the circumflex ($\hat{}$), and the solenoidal variables by the tilde ($\tilde{}$), we express the time-dependent quantities as

$$\omega^{(1)}\equiv\nabla\times\mathbf{u}^{(1)}=\tilde{\omega}\equiv\nabla\times\tilde{\mathbf{u}}, \tag{17}$$

$$p^{(1)}=\hat{p}, \tag{18}$$

$$\rho^{(1)}=\hat{\rho}, \tag{19}$$

where vorticity is produced exclusively by the rotational mode and acoustic pressure is caused predominantly by the irrotational pressure mode. The pseudo-pressure generated by the vortical mode is ignored, being of second order in the wave amplitude.[9]

B. Time-dependent equations of motion

Substituting Eqs. (16)–(19) into the first order time-dependent set, given by Eqs. (10)–(11), yields the following two independent sets that are coupled through existing boundary conditions:

1. Acoustical model

$$\partial\hat{\rho}/\partial t+\nabla\cdot\hat{\mathbf{u}}=-M_b\nabla\cdot(\hat{\rho}\mathbf{U}), \tag{20}$$

$$\frac{\partial\hat{\mathbf{u}}}{\partial t}=-\frac{\nabla\hat{p}}{\gamma}-M_b\nabla(\hat{\mathbf{u}}\cdot\mathbf{U})+\frac{4\nabla(\nabla.\hat{\mathbf{u}})}{3\,\mathrm{Re}}. \tag{21}$$

2. Vortical model

$$\nabla\cdot\tilde{\mathbf{u}}=0, \tag{22}$$

$$\frac{\partial\tilde{\mathbf{u}}}{\partial t}=M_b[\mathbf{U}\times\tilde{\omega}-\nabla(\tilde{\mathbf{u}}\cdot\mathbf{U})]-\frac{\nabla\times\tilde{\omega}}{\mathrm{Re}}. \tag{23}$$

C. Auxiliary conditions

In order to determine the total time-dependent velocity $\mathbf{u}^{(1)}$, irrotational and vortical components have to be determined separately by solving Eqs. (20)–(21), and Eqs. (22)–(23). Resulting solutions must be superimposed in a manner to correctly satisfy two existing boundary conditions: (1) Velocity adherence at the wall demanding the axial time-dependent component of the velocity to vanish at $y=1$, thus yielding $\tilde{u}_z(1,z)=-\hat{u}_z(1,z)$, and (2) symmetry at $y=0$, giving $\partial u^{(1)}(0,z)/\partial y=0$.

D. Irrotational solution

Equations (20)–(21) can be cast into a second order hyperbolic partial differential equation (PDE), namely,

$$\frac{\partial^2 \hat{p}}{\partial t^2} - \nabla^2 \hat{p} = -M_b \left[\nabla . \left(\frac{\partial \hat{p}}{\partial t} \mathbf{U} \right) + \gamma \nabla^2 (\hat{\mathbf{u}} . \mathbf{U}) \right], \tag{24}$$

which can be solved to the first order in the Mach number by separation of variables. Following similar arguments to those presented in Ref. 1, the solution for the acoustic pressure $\hat{p}(z,t)$ can be expressed as

$$\hat{p}(z,t) = \epsilon_w \cos(k_m z) \exp(-ik_m t), \tag{25}$$

where the dimensionless wave number is given by $k_m = m\pi H/L$, $m = 1,2,3,...$, and m is the acoustic mode number. The acoustic velocity companion is determined directly from the momentum conservation Eq. (21) of order M_b. The result is

$$\hat{\mathbf{u}}(z,t) = i \frac{\epsilon_w}{\gamma} \sin(k_m z) \exp(-ik_m t) \mathbf{e}_z . \tag{26}$$

Note that both z and t are dimensionless quantities, as explained in Sec. II A.

E. Fundamental vortical equations

Using Euler's notation, we express rotational velocity and vorticity components in the following fashion:

$$\tilde{\mathbf{u}}(y,z,t) = \mathbf{V}(y,z) \exp(-ik_m t), \tag{27}$$

$$\tilde{\boldsymbol{\omega}}(y,z,t) = \overline{\boldsymbol{\omega}}(y,z) \exp(-ik_m t), \tag{28}$$

where

$$\mathbf{V}(y,z) = V_y \mathbf{e}_y + V_z \mathbf{e}_z , \tag{29}$$

$$\overline{\boldsymbol{\omega}} = \nabla \times \mathbf{V} = \overline{\omega} \mathbf{e}_x \tag{30}$$

are complex functions. It follows that the vortical mass and momentum conservation equations, given by Eqs. (22)–(23), become

$$\nabla . \mathbf{V} = 0, \tag{31}$$

$$i\mathbf{V} = \sigma [\nabla (\mathbf{V}.\mathbf{U}) - \mathbf{U} \times \overline{\boldsymbol{\omega}}] + \epsilon \nabla \times \overline{\boldsymbol{\omega}}, \tag{32}$$

where

$$\sigma = \frac{M_b}{k_m} = \frac{1}{Sr} = \frac{V_b}{\omega_0 H} < O(10^{-1}), \tag{33}$$

$$\epsilon = \frac{1}{k_m \, \mathrm{Re}} = \frac{1}{\mathrm{Re}_k} = \left(\frac{\sqrt{\nu_0 / \omega_0}}{H} \right)^2 < O(10^{-4}) \tag{34}$$

are naturally occurring dimensionless groupings representing the reciprocals of the Strouhal and kinetic Reynolds numbers, and satisfying

$$\epsilon / \sigma = \nu_0 / (V_b H) \ll 1. \tag{35}$$

Indubitably, $\mathrm{Re}_k = 2\lambda_S^2$ is another form of the Stokes number, λ_S, which is expected to play a nontrivial role in oscillatory flows. Equations (31)–(32) can be expanded in scalar form into

$$\frac{\partial V_y}{\partial y} + \frac{\partial V_z}{\partial z} = 0, \tag{36}$$

$$iV_y = \sigma \left[\frac{\partial}{\partial y} (V_y U_y) + U_z \frac{\partial V_y}{\partial z} + V_z \frac{\partial U_y}{\partial z} \right] - \epsilon \left(\frac{\partial^2 V_y}{\partial z^2} - \frac{\partial^2 V_z}{\partial y \partial z} \right), \tag{37}$$

$$iV_z = \sigma \left[\frac{\partial}{\partial z} (V_z U_z) + U_y \frac{\partial V_z}{\partial y} + V_y \frac{\partial U_z}{\partial y} \right] - \epsilon \left(\frac{\partial^2 V_z}{\partial y^2} - \frac{\partial^2 V_y}{\partial y \partial z} \right), \tag{38}$$

which reveal that direct analytical solutions to the coupled set are not tractable without exploitation of an important result that can be verified numerically, and proven theoretically, only *a posteriori*. Subject to later verification, the normal vortical velocity V_y is assumed to be of $O(M_b)$ by comparison to the axial component V_z. Being a smaller quantity, ignoring V_y at the first perturbation expansion level of V will not affect the solution which, let us recall, is only accurate to the first order in the Mach number. On that account, Eq. (38) becomes

$$iV_z = \sigma \left[\frac{\partial}{\partial z} (V_z U_z) + U_y \frac{\partial V_z}{\partial y} \right] - \epsilon \frac{\partial^2 V_z}{\partial y^2} + O(M_b). \tag{39}$$

V. VORTICAL SOLUTION

Using separation of variables, a careful scaling analysis, and two-variable multiple scale expansions, an explicit solution to the solenoidal velocity component is sought.

A. Separation of variables

Inserting Eq. (12) into Eq. (39), expanding and rearranging, one gets

$$z \frac{\partial V_z}{\partial z} = \left(\frac{i}{\sigma} - 1 \right) V_z + y \frac{\partial V_z}{\partial y} + \frac{\epsilon}{\sigma} \frac{\partial^2 V_z}{\partial y^2}, \tag{40}$$

which suggests using separation of variables in order to investigate a solution of the type

$$V_z(y,z) = Y(y) Z(z). \tag{41}$$

When inserted back into Eq. (40), Eq. (41) allows splitting the original PDE into two linear ordinary differential equations (ODEs), coupled through a separation constant λ_n:

$$\frac{z}{Z} \frac{dZ}{dz} = \left(\frac{i}{\sigma} - 1 \right) + \frac{y}{Y} \frac{dY}{dy} + \frac{\epsilon}{\sigma} \frac{d^2 Y}{dy^2} = \lambda_n , \tag{42}$$

where λ_n must be strictly positive for a nontrivial outcome. For every λ_n, a solution Z_n and Y_n are manageable. Integration of the axially dependent equation is straightforward. The exact result is $Z_n(z) = c_n z^{\lambda_n}$, where c_n is an integration constant associated with λ_n. Since the governing equation is linear, any linear combination of two or more solutions is also a solution, and one can write, in general, for all possible λ_n

$$V_z(y,z)=\sum_{\lambda_n} c_n z^{\lambda_n} Y_n(y), \tag{43}$$

where λ_n must be determined from the no-slip boundary condition at the wall giving rise to the strong coupling between pressure and vorticity modes. As a consequence, rotational and irrotational components of the axial velocity cancel out at $y=1$. This is achieved when $\tilde{\mathbf{u}}_z=-\hat{\mathbf{u}}_z$, or

$$V_z(1,z)=-(\epsilon_w/\gamma)i\sin(k_m z). \tag{44}$$

Inserting Eq. (44) into Eq. (43), writing out the MacLaurin series expansion for the Sine function, and equating summation terms lead to

$$\sum_{\lambda_n} c_n z^{\lambda_n} Y_n(1)\equiv -\frac{\epsilon_w}{\gamma} i\sum_{n=0}^{\infty}\frac{(-1)^n (k_m z)^{2n+1}}{(2n+1)!}, \tag{45}$$

which holds true when $\lambda_n=2n+1$, $n=0,1,...$, and

$$c_n=-\frac{\epsilon_w}{\gamma} i\frac{(-1)^n (k_m)^{2n+1}}{(2n+1)!}, \tag{46}$$

$$Y_n(1)=1, \tag{47}$$

turning Eq. (43) into

$$V_z(y,z)=-\frac{\epsilon_w}{\gamma} i\sum_{n=0}^{\infty}\frac{(-1)^n (k_m z)^{2n+1}}{(2n+1)!} Y_n(y). \tag{48}$$

In order to satisfy Eq. (42), the velocity eigenfunction $Y_n(y)$ remains to be determined from the two-point boundary value problem prescribed by

$$\epsilon\frac{d^2Y_n}{dy^2}+\sigma y\frac{dY_n}{dy}+[i-(1+\lambda_n)\sigma]Y_n=0, \tag{49}$$

a second order ODE that is constrained by two naturally occurring auxiliary conditions:

$$Y_n(1)=1 \quad \text{(no-slip)}, \tag{50}$$

$$\frac{dY_n(0)}{dy}=0 \quad \text{(axial symmetry)}. \tag{51}$$

Equation (49) exhibits a practical closed form solution following a careful application of the derivative expansion method. This approach is presented next.

B. Scaling analysis

The first step for the derivative expansion method to work is the judicious identification of the scale at which order balance is achieved between locally significant terms in the governing ODE. To that end, we make the conjecture that, near the regular singularity

$$y=\epsilon^{1/q} y_1^{-1/q}, \tag{52}$$

where y_1 is the relevant local scale and q is a stretching exponent that must be carefully determined. The derivatives become

$$\frac{dY_n}{dy}=-q\epsilon^{-1/q} y_1^{1+1/q}\frac{dY_n}{dy_1}, \tag{53}$$

$$\frac{d^2Y_n}{dy^2}=q\epsilon^{-2/q} y_1^{1+2/q}\left[q y_1\frac{d^2Y_n}{dy_1^2}+(q+1)\frac{dY_n}{dy_1}\right]. \tag{54}$$

Substituting back into Eq. (49), we get

$$\epsilon^{1-2/q} q^2 y_1^{2+2/q}\frac{d^2Y_n}{dy_1^2}+q y_1[\epsilon^{1-2/q}(q+1)y_1^{2/q}-\sigma]\frac{dY_n}{dy_1}+[i-(1+\lambda_n)\sigma]Y_n=0, \tag{55}$$

which clearly indicates that $q=2$ is a key stretching exponent that corresponds to a distinct limit for which balance between various terms in Eq. (55) will exist. The rescaled equation becomes

$$4y_1^3\frac{d^2Y_n}{dy_1^2}+2y_1(3y_1-\sigma)\frac{dY_n}{dy_1}+[i-(1+\lambda_n)\sigma]Y_n=0, \tag{56}$$

where the modified scale is

$$y_1=\epsilon y^{-2}. \tag{57}$$

Thus when $y=O(\epsilon^{1/2})$, representing the characteristic thickness of the inner layer near $y=0$, the new variable y_1 will be of $O(1)$, which allows resolving accurately the rapid changes that can occur in such a small interval.

C. Two-variable multiple-scale expansions

Having determined the form of the inner scale, a standard multiple-scale procedure can be implemented to transform Eq. (49) into a PDE that is function of two virtual variables, $y_0=y$, and $y_1=\epsilon y^{-2}$. This requires expanding the derivatives in terms of the new variables

$$\frac{d}{dy}=\frac{\partial}{\partial y_0}\frac{dy_0}{dy}+\frac{\partial}{\partial y_1}\frac{dy_1}{dy}=\frac{\partial}{\partial y_0}-2\epsilon y_0^{-3}\frac{\partial}{\partial y_1}, \tag{58}$$

$$\frac{d^2}{dy^2}=\frac{\partial^2}{\partial y_0^2}+O(\epsilon). \tag{59}$$

Note that the current choice of an inner scale represents a minor departure from the conventional form of y/ϵ^{λ}, including $y_1=y/\sqrt{\epsilon}$, which would be ordinarily attempted by a skilled perturbation proponent. The latter form, recommended by most books on the subject, does not lead to a meaningful solution in the case at hand. Substituting Eqs. (58)–(59) back into Eq. (49), we obtain the following PDE:

$$\epsilon\frac{\partial^2 Y_n}{\partial y_0^2}+\sigma y_0\left(\frac{\partial Y_n}{\partial y_0}-2\epsilon y_0^{-3}\frac{\partial Y_n}{\partial y_1}\right)+[i-\sigma(1+\lambda_n)]Y_n+O(\epsilon^2)=0. \tag{60}$$

Next, Y_n is expanded as a sum consisting of a leading order term and a series of consistently decreasing terms:

$$Y_n=Y_n^{(0)}+\epsilon Y_n^{(1)}+O(\epsilon^2), \tag{61}$$

where $Y_n^{(0)}$ is the leading order term that we propose to find. Inserting the two-term expansion of Y_n into Eq. (60), rearranging and collecting terms of $O(1)$ and $O(\epsilon)$, we get, respectively,

$$\epsilon^0: \quad \sigma y_0 \frac{\partial Y_n^{(0)}}{\partial y_0} + [i-(1+\lambda_n)\sigma] Y_n^{(0)} = 0, \tag{62}$$

$$\epsilon: \quad \sigma y_0 \frac{\partial Y_n^{(1)}}{\partial y_0} + [i-(1+\lambda_n)\sigma] Y_n^{(1)} = 2\sigma y_0^{-2} \frac{\partial Y_n^{(0)}}{\partial y_1} - \frac{\partial^2 Y_n^{(0)}}{\partial y_0^2}. \tag{63}$$

Partial integration of Eq. (62) gives $Y_n^{(0)}$:

$$Y_n^{(0)}(y_0, y_1) = C_1(y_1) \exp\{[(1+\lambda_n) - i/\sigma] \ln y_0\}, \tag{64}$$

where the constant of integration C_1 can, in general, be a function of y_1; following traditional multiple-scale arguments, C_1 must be determined in a manner to ensure that $Y_n^{(0)}$ remains uniformly valid, viz., $Y_n^{(0)} > \epsilon Y_n^{(1)}, \forall y$. This will occur when the first order term in Eq. (61) remains smaller that the leading order term in the series expansion for all y. This can only happen when the right hand side of Eq. (63) is zero. Differently stated, if the right hand side of Eq. (63) is not zero, the solution for $Y_n^{(1)}$ will include what is known in perturbation theory as ''secular'' terms. These are undesirable terms that make $Y_n^{(1)}$, in some regions of the solution domain, grow until $\epsilon Y_n^{(1)}$ exceeds $Y_n^{(0)}$. Evidently, this condition cannot be tolerated since it violates the original premise and, furthermore, invalidates the regular perturbation expansion of Y_n in a series of decreasing order terms. To suppress the source of secular terms, we set

$$2\sigma y_0^{-2} \frac{\partial Y_n^{(0)}}{\partial y_1} - \frac{\partial^2 Y_n^{(0)}}{\partial y_0^2} = 0, \tag{65}$$

where the derivatives are

$$\frac{\partial Y_n^{(0)}}{\partial y_1} = \frac{dC_1}{dy_1} \frac{Y_n^{(0)}}{C_1}, \tag{66}$$

$$\frac{\partial^2 Y_n^{(0)}}{\partial y_0^2} = (\lambda_n - i/\sigma)[(1+\lambda_n) - i/\sigma] \frac{Y_n^{(0)}}{y_0^2}, \tag{67}$$

which, when substituted back into Eq. (65), yield

$$\frac{dC_1}{dy_1} - \frac{(\lambda_n - i/\sigma)[(1+\lambda_n) - i/\sigma]}{2\sigma} C_1 = 0, \tag{68}$$

which can be easily solved for C_1:

$$C_1 = C_0 \exp\left\{ \frac{(\lambda_n - i/\sigma)[(1+\lambda_n) - i/\sigma]}{2\sigma} y_1 \right\}. \tag{69}$$

Recalling that $y_1 = \epsilon y^{-2}$, the general, uniformly valid solution for Y_n is

$$Y_n(y) = C_0 \exp\left\{ [(1+\lambda_n) - i/\sigma] \ln y + \frac{\epsilon(\lambda_n - i/\sigma)[(1+\lambda_n) - i/\sigma]}{2\sigma y^2} \right\} + O(\epsilon), \tag{70}$$

where C_0 can be determined readily from Eq. (50). Subsequently,

$$Y_n(y) = y^{(1+\lambda_n)} \exp\{-\xi[1-\sigma^2\lambda_n(1+\lambda_n)](y^{-2}-1)/2 - i[\ln y + \xi\sigma^2(1+2\lambda_n)(y^{-2}-1)/2]/\sigma\} + O(\epsilon), \tag{71}$$

where $\xi = \epsilon/\sigma^3$ is a nondimensional parameter that has a strong influence on the damping rate of Y_n.

D. Analytical solution in infinite series form

Employing Eq. (71) in Eq. (48), letting $\eta = (y^{-2}-1)/2$ for convenience, and summing up over all possible λ_n, renders

$$V_z(y,z) = -\frac{\epsilon_w}{\gamma} i \sum_{n=0}^{\infty} \frac{(-1)^n (k_m z)^{2n+1}}{(2n+1)!} y^{(2n+2)} \times \exp\{-[1-\sigma^2(2n+1)(2n+2)]\xi\eta - i[\ln y + \xi\sigma^2(4n+3)\eta]/\sigma\} + O(\epsilon). \tag{72}$$

From Eq. (27), $\tilde{u}_z$ can be written in an infinite series form that clearly displays the leading order quantities and smaller quantities of $O(\sigma^2)$:

$$\tilde{u}_z(y,z,t) = -\frac{\epsilon_w}{\gamma} iy \sum_{n=0}^{\infty} \frac{(-1)^n (k_m yz)^{2n+1}}{(2n+1)!} \times \exp\{-[1-\sigma^2(2n+1)(2n+2)]\xi\eta - i[\ln y + \xi\sigma^2(4n+3)\eta]/\sigma - ik_m t\} + O(\epsilon). \tag{73}$$

Fortunately, Eq. (73) is a rapidly converging series.

E. Accurate closed form equivalent

Equation (73) can be written in a closed form by disregarding small terms that do not affect the order of the error associated with the infinite series itself. The result is a practical, closed form equivalent

$$\tilde{u}_z(y,z,t) = -\frac{\epsilon_w}{\gamma} iy \sin(k_m yz) \exp[-(1-2\sigma^2)\xi\eta - i(\ln y + 3\xi\sigma^2\eta)/\sigma - ik_m t] + O(\epsilon). \tag{74}$$

F. Graphical verification

In order to verify that Eqs. (73) and (74) are concurrent, we first construct a solution for $\mathbf{u}^{(1)}$ by adding the irrotational component to $\tilde{u}_z$ in Eq. (59). This can be accomplished using either one of the two versions represented by Eqs. (73) and (74). In either case, the penetration depth δ of the resulting time-dependent velocity can be evaluated and compared to a reliable numerical solution to Eq. (39) achieved using a Runge–Kutta scheme of order seven.[12] In Fig. 3, a typical example is furnished that illustrates the excellent agreement between analytical predictions for $\tilde{u}_z$ and the numerical solution to Eq. (23). Since locating δ is sensitive to error accumulation, we overlay analytical predictions of δ vs σ in Fig. 4 for a wide range of physical parameters as obtained from Eqs. (73) and (74). Reassuringly, no discernible discrepancies are detected anywhere, indicating that Eq. (74) can be

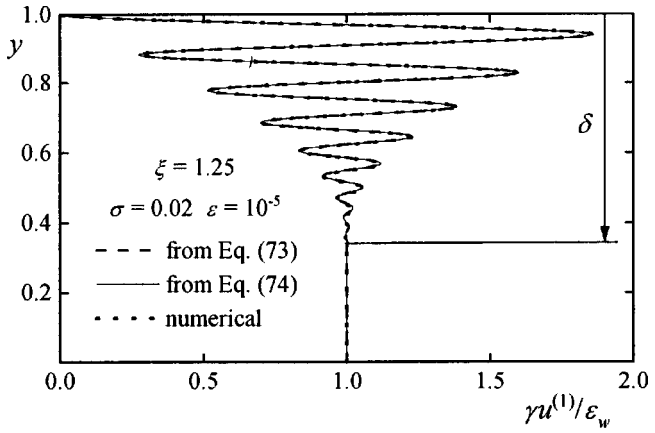

FIG. 3. Virtually indistinguishable results for the total time-dependent velocity at chamber midspan as predicted from numerical, infinite series, and closed form expressions corresponding to Eqs. (73) and (74).

exchanged for Eq. (73) without any appreciable loss in accuracy. This conclusion can be further confirmed by running a standard error calculation.

In addition to its simplicity and remarkable precision, Eq. (74) discloses the leading order terms which control the solution. These relate to the convection of unsteady vorticity by the mean flow in both axial and normal directions, time-dependent inertia, and viscous diffusion of time-dependent vorticity.

G. Normal velocity

The normal component $\tilde{u}_y$ can be determined in a manner to satisfy continuity. To that end, $\tilde{u}_z$ is used in Eq. (22) while a guessed function is proposed for $\tilde{u}_y$. From a conjectured form

$$\tilde{u}_y(y,z,t)=\frac{\epsilon_w}{\gamma}G(y)\cos(k_m yz)\exp[-(1-2\sigma^2)\xi\eta - i(\ln y+3\xi\sigma^2\eta)/\sigma - ik_m t]+O(\epsilon), \quad (75)$$

the unknown function $G(y)$ must be determined to satisfy continuity. Substituting Eq. (74) and Eq. (75) into Eq. (22), the spatial function $G(y)$ is extracted in a manner to ensure that $\partial\tilde{u}_y/\partial y=-\partial\tilde{u}_z/\partial z$ is satisfied in the leading order terms. This occurs when

$$G(y)=-M_b y^3, \quad (76)$$

rendering

$$\tilde{u}_y(y,z,t)=-\frac{\epsilon_w}{\gamma}M_b y^3\cos(k_m yz)\exp[-(1-2\sigma^2)\xi\eta - i(\ln y+3\xi\sigma^2\eta)/\sigma - ik_m t]+O(\epsilon). \quad (77)$$

Clearly, the original assumption of $\tilde{u}_y/\tilde{u}_z=O(M_b)$—leading to Eq. (39)—is justifiable. Furthermore, numerical computations of $\tilde{u}_y$ indicate that Eq. (77) is indeed accurate. Such comparisons with numerical predictions of $\tilde{u}_y$ are excluded here for brevity.

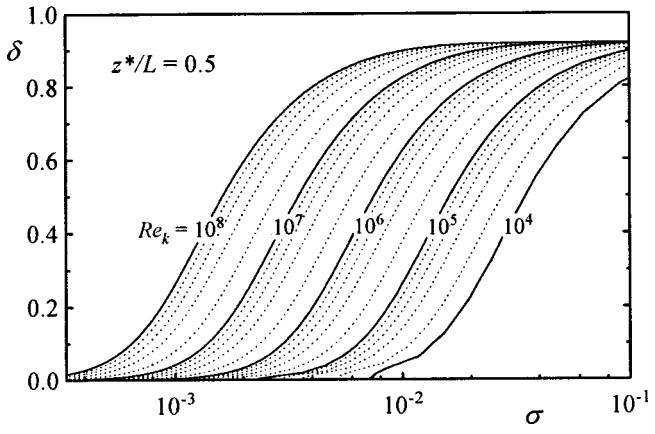

FIG. 4. Penetration depth predictions from infinite series and closed form expressions, viz., Eqs. (73) and (74). To the accuracy of the graph, differences between both formulations cannot be distinguished. Broken lines of constant Re_k are equally spaced.

VI. SOLUTION CHARACTER

The behavior and character of the time-dependent velocity can now be examined along with its accompanying boundary layer structure. The global error associated with the analytical outcome can also be evaluated to confirm theoretical predictions.

A. Total time-dependent velocity

Superimposing rotational and irrotational velocity fields in Eq. (16), $u_z^{(1)}$ can be formulated at $O(M_b)$:

$$u_z^{(1)}(y,z,t)=\frac{\epsilon_w}{\gamma}i\exp(-ik_m t)\{\sin(k_m z)-y\sin(k_m yz)\times\exp[-(1-2\sigma^2)\xi\eta - i(\ln y+3\xi\sigma^2\eta)/\sigma]\}, \quad (78)$$

whose real part is

$$u_z^{(1)}(y,z,t)=\frac{\epsilon_w}{\gamma}\Bigg[\overbrace{\sin(k_m z)\sin(k_m t)}^{\text{acoustic part}} \underbrace{\overbrace{-y\sin(k_m yz)\exp(-\zeta)}^{\text{solenoidal amplitude}}\ \overbrace{\sin(k_m t+\Phi)}^{\text{wave propagation}}}_{\text{solenoidal part}}\Bigg], \quad (79)$$

where

$$\zeta=\xi(1-2\sigma^2)(y^{-2}-1)/2, \quad (80)$$

$$\Phi=[\ln y+3\xi\sigma^2(y^{-2}-1)/2]/\sigma. \quad (81)$$

Evidently, $u^{(1)}$ is prescribed by $u_z^{(1)}$ which is a harmonic wave that proceeds from the wall ($y=0$) and travels in the direction of increasing y. It is characterized by a wave amplitude that diminishes exponentially with increasing distance from the wall. The decay constant associated with the exponential decrease can be extrapolated by inspecting Eqs. (79)–(80) to be the viscosity parameter ξ. The vortical wave amplitude is actually controlled by two terms: an exponentially decaying term, made possible by inclusion of viscous dissipation (i.e., ζ), that decreases with the distance from the

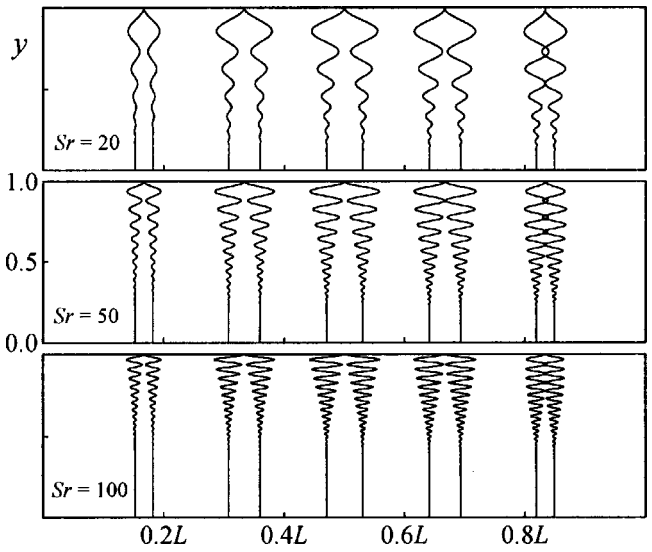

FIG. 5. Time-dependent velocity patterns shown at several axial stations for $\mathrm{Re}_k=10^6$ and typical values of the Strouhal number.

wall, and a sinusoidal term, made possible by inclusion of axial mean flow convection of unsteady vorticity, which varies harmonically with the distance from the head end, and also decreases with the distance from the wall. By inspection of the spatial damping function ζ in Eq. (74) and Eq. (79), increasing viscosity is found to cause the rotational wave to decay more rapidly, preventing a deeper inward penetration of vorticity. This effect is contrary to the boundary-layer ''thickening'' role played by viscosity in oscillatory flows between parallel rigid walls. Incorporation of blowing effects appears to alter the flow character quite dramatically. Results from Eq. (79) are congruent with numerical predictions which are achieved to a high order of accuracy (using a step size of 10^{-6} in conjunction with a nine-stage Runge–Kutta scheme that exhibits a global error of order seven).[12] This agreement, shown in Fig. 5, causes differences in graphical results to become visually indiscernible.

When, in Fig. 5, numerical and analytical velocity distributions are overlaid, no appreciable discrepancies can be perceived. Local velocity profiles shown correspond to instantaneous profiles separated by 180 degrees of a full oscillation cycle depicted at several axial locations for the fundamental pressure oscillation mode. Note that the solenoidal component of the velocity is more pronounced in the downstream portions of the cavity where time-dependent vorticity is intensified. The figure also indicates that the spatial wavelength of solenoidal waves diminishes at higher Strouhal numbers.

B. Acoustic boundary layer

We start by examining the rotational wave amplitude which controls the evolution of the time-dependent boundary-layer envelope:

$$\|\tilde{u}^{(1)}\|=\frac{\epsilon_w}{\gamma}y\,\sin(k_m yz)\exp[-(1-2\sigma^2)\xi\eta]. \tag{82}$$

Defining the boundary layer to extend from the compliant wall to the point where 99% of the rotational wave component has vanished, the corresponding boundary layer thickness will be the distance from the wall to the point where $\|\tilde{u}^{(1)}\|$ becomes $\alpha\equiv 1\%$ of its irrotational counterpart. The normalized penetration depth δ extending from the wall to the edge of the boundary layer can, therefore, be calculated from $y_p=1-\delta$, where

$$y_p\sin(k_m y_p z)\exp[-(1-2\sigma^2)\xi\eta]-\alpha|\sin(k_m z)|=0. \tag{83}$$

Plots of δ vs σ for a wide range of Re_k are shown in Fig. 6 at two axial stations that are 5% of the longitudinal length from each end: one near the head end ($z^*=0.05L$) and the other near the aft end ($z^*=0.05L$). The wide spread in the data makes it difficult to interpret the dependence of δ on actual physical parameters. This problem is alleviated by referring to Eq. (83) which clearly shows that the term involving exponential boundary layer decay is a strong function of a viscous damping parameter, ξ. This subtle realization motivates generating curves of δ vs ξ, for wide variations in Re_k. As shown in Fig. 7, entire families of curves, such as those shown in Fig. 4 (for $z^*=0.5L$) and Fig. 6 at discrete axial

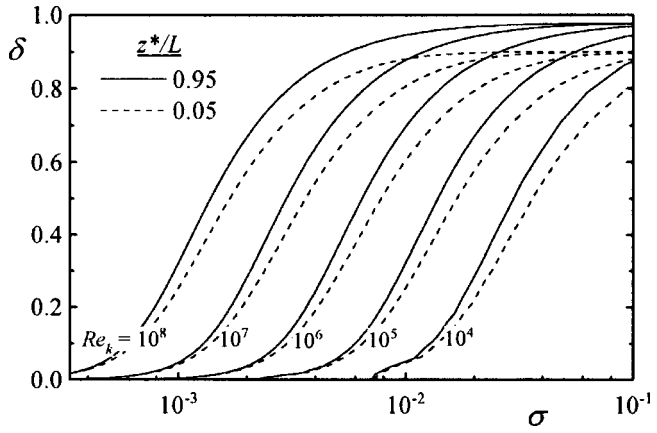

FIG. 6. Locus of the rotational boundary-layer thickness at two axial stations and $m=1$. Since δ grows from the head end, the upper family of curves (solid lines) corresponds to the downstream location.

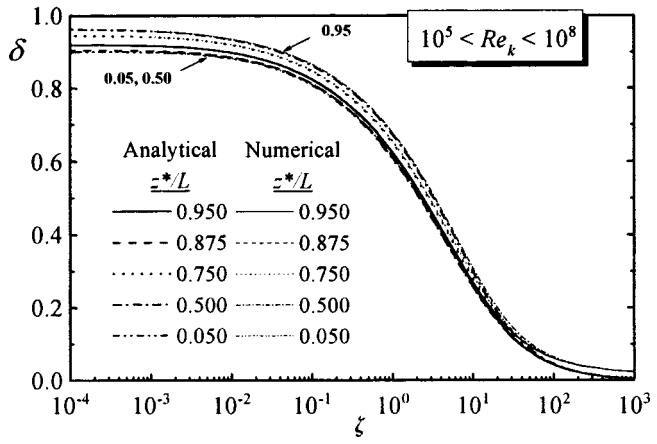

FIG. 7. The boundary-layer thickness determined numerically and analytically at five discrete locations. To the resolution of this graph, no changes in δ seem to occur in the cavity's forward half portion ($0.05\leqslant z^*/L\leqslant 0.5$). Except for large ξ, differences between numerical and analytical predictions are hardly noticeable.

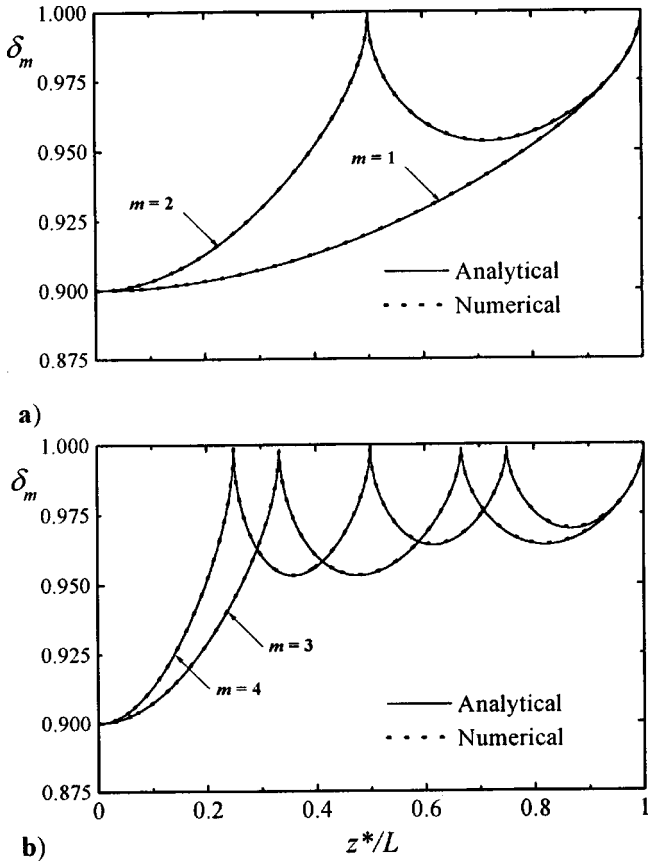

FIG. 8. Trace of the maximum boundary-layer thickness corresponding to ideal fluids and the first four acoustic modes: (a) $m=1,2$ and (b) $m=3,4$.

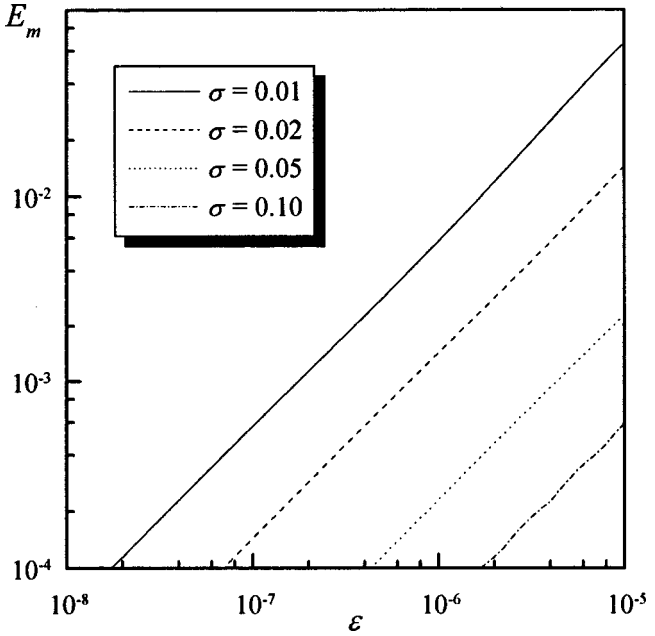

FIG. 9. Maximum absolute error.

stations, collapse splendidly into single curves per axial location. This significant result reveals that δ does not depend on Re_k and σ separately, but rather on $\xi=\omega_0^2 v_0 H V_b^{-3}$, a key similarity parameter that resembles, in importance, the Stokes number in oscillating flows over nontranspiring walls. However, unlike many similarity parameters, ξ cannot be disclosed by standard dimensional analysis.

Figures 7 and 8 bring into focus the character of the boundary-layer thickness over permeable walls that is defined in Fig. 3. For instance, it is clear from Eq. (83) that $\delta=f(\xi,m,z)$ must depend on ξ, the pressure mode number and, to a lesser degree, on the axial station within the chamber. For the fundamental pressure oscillation mode, $m=1$, Fig. 7 shows that, for large ξ, δ varies linearly with ξ, independently of z. Smaller ξ imply larger penetration depths due to a smaller argument in the exponentially decaying term. Furthermore, increasing the blowing speed, or decreasing viscosity, frequency, or chamber height seems to enhance the depth of penetration. Eventually, for sufficiently small ξ, δ tends asymptotically to a maximum fixed value per axial position. This maximum fixed value becomes independent of ξ and the corresponding depth becomes $\delta=f(m,z)$ as $\xi\rightarrow 0$.

In order to pinpoint this maximum possible penetration depth, δ_m, occurring per axial station and mode number, we realize that, for the same geometry and blowing speed, larger penetration occurs in fluids with smaller viscosity. In the ideal case of zero viscosity, rotational waves face minimum friction and, thereby, travel the furthest distance from the wall. The asymptotic limit on the thickness of the boundary layer can thus be determined from the inviscid formulation of the penetration depth—which only depends on the axial station z and pressure mode m. Setting $v_0=0$ or $\xi=0$ in Eq. (83), we get

$$(1-\delta_m)\sin[k_m(1-\delta_m)z]-\alpha|\sin(k_m z)|=0. \tag{84}$$

The resulting expansion formula is

$$\delta_m=1-\sqrt{\alpha|\sin(k_m z)|/(k_m z)}+O(1-\delta_m)^4, \tag{85}$$

which allows predicting the inviscid depth of penetration quite accurately. A maximum truncation error of $O(10^{-4})$ corresponds to the smallest value of δ_m, which is 0.9 for $z=0$. Having a smaller truncation error than $O(M_b)$, Eq. (85) can be exchanged for the numerical solution to Eq. (84). This is illustrated in Fig. 8 below for the first four acoustic modes where δ_m is shown to vary between 90% and 100% of the solution domain.

C. Global error analysis

In order to ensure that no mistakes were committed in the derivation process, and to verify the order of the error associated with the final expression for the time-dependent velocity field, viz., Eq. (79), we calculate the maximum absolute error E_m between the analytical prediction and the numerical outcome of Eq. (11) following Bosley's constructive recommendation.[13] Since the absolute error defined here represents the deviation from the numerical solution, the latter is determined very accurately by using a seventh order Runge–Kutta scheme and a subinterval of 10^{-6}. Assuming that the maximum absolute error exhibits the classical form

$$E_m=|u^{(1)}_{\text{numerical}}-u^{(1)}_{\text{analytical}}|_{\max}=K\epsilon^{\kappa}, \tag{86}$$

then the order of the error, κ, can be determined from the slope of the linear least-squares (LS) fit to the data set generated by plotting $\lg E_m$ vs $\lg \epsilon$ for different values of σ. As it can be inferred from Fig. 9, the order of the error κ is about unity. Linear slopes obtained from LS lines with high correlation coefficients confirm that, indeed, κ varies from 0.99 to 0.999 999 in decreasing ranges of ϵ. In fact, regardless of σ, we can write with confidence that

$$\kappa \xrightarrow[\epsilon \to 0]{} 1. \tag{87}$$

This reassuring observation leads us to conclude that the error associated with Eq. (79) is of $O(\epsilon)$.

VII. CONCLUSIONS

In this article, the oscillatory field that results from harmonic pressure disturbances superimposed on the mean flow inside a rectangular cavity is resolved using asymptotics. With regard to the time-dependent field, accurate expressions for the axial and normal velocity components are extracted. The normal velocity is found to be small, namely, of the order of the surface Mach number, by comparison to the axial counterpart. The latter dictates its character in the total solution which represents a traveling wave that decays with distance from the wall. The rate of decay is found to be a strong function of a nondimensional parameter, $\xi = \omega_0^2 \nu_0 H V_b^{-3}$, that has a profound impact on the solution. This so-called viscosity parameter combines both Strouhal and kinetic Reynolds numbers via $\xi = \mathrm{Sr}^3/\mathrm{Re}_k$. This dimensionless grouping appears in the analytical formulation to be the primary similarity parameter in control of the solution. At the outset, large viscosity leads to faster attenuation of the traveling wave envelope, and thereby, to smaller penetration depths of rotational waves. In addition to its strong dependence on ξ, the penetration depth of rotational waves is found to depend on the acoustic mode number m, and on the distance from the head end, z. An accurate expansion formula is extracted for the maximum penetration depth associated with ideal fluids with small viscosity. Finally, a standard analysis of the maximum error associated with the analytical derivation validates the rigor of the perturbation approach and confirms the order of the reported truncation error. Experimental verification remains to be addressed in a forthcoming article.

[1] J. Majdalani and W. K. Van Moorhem, ''Improved time-dependent flow field solution for solid rocket motors,'' AIAA J. **36**, 241–248 (1998).
[2] Y. Ma, ''A simulation of the flow near a burning propellant in a solid propellant rocket motor,'' Ph. D. dissertation, University of Utah (1990).
[3] Y. Ma, W. K. Van Moorhem, and R. W. Shorthill, ''Innovative method of investigating the role of turbulence in the velocity coupling phenomenon,'' Journal of Vibration & Acoustics-Transactions of the ASME **112**, 550–555 (1990).
[4] Y. Ma, W. K. Van Moorhem, and R. W. Shorthill, ''Experimental investigation of velocity coupling in combustion instability,'' J. Propul. Power **7**, 692–699 (1991).
[5] J. Barron, ''The onset of turbulence in a simulation of the oscillating flow over a burning propellant,'' Ph.D. dissertation, University of Utah (1997).
[6] M. Van Dyke, *Perturbation Methods in Fluid Mechanics* (The Parabolic Press, Stanford, CA, 1975).
[7] F. M. White, *Viscous Fluid Flow* (McGraw-Hill, New York, 1991), p. 153.
[8] A. Sommerfeld, *Mechanics of Deformable Bodies* (Academic, New York, 1950), p. 147.
[9] B. T. Chu and L. S. G. Kovásznay, ''Nonlinear interactions in a viscous heat-conducting compressible gas,'' J. Fluid Mech. **3**, 494–514 (1957).
[10] B. T. Carrier and F. D. Carlson, ''On the propagation of small disturbances in a moving compressible fluid,'' Q. Appl. Math. **4**, 1–12 (1946).
[11] G. A. Flandro, ''Solid propellant acoustic admittance corrections,'' J. Sound Vib. **36**, 297–312 (1974).
[12] J. C. Butcher, *The Numerical Analysis of Ordinary Differential Equations* (Wiley, Great Britain, 1987).
[13] D. L. Bosley, ''A technique for the numerical verification of asymptotic expansions,'' SIAM (Soc. Ind. Appl. Math.) Rev. **38**, 128–135 (1996).